Navier-Stokes Calculations Using Cartesian Grids: I. Laminar Flows

Paul D. Frymier Jr.* and H. A. Hassan†
North Carolina State University, Raleigh, North Carolina
and
M. D. Salas‡
NASA Langley Research Center, Hampton, Virginia

A finite-volume formulation for the Navier-Stokes equations using Cartesian grids is used to study flows past airfoils. In addition to the solution of the complete equations, solutions for two simplified versions of the governing equations were obtained and compared with those using body-fitted grids. Results are presented for two airfoil sections, NACA 0012 and RAE 2822, for a range of Mach numbers, angles of attack, and Reynolds numbers. It is shown that the results are highly dependent on the smoothness of the surface grid. Without such smoothness, the skin friction and pressure converge to nonuniform distributions. On the other hand, when surface cells with smoothly varying areas are used, the results compare favorably with calculations employing body-fitted grids.

Introduction

CURRENTLY, much of the work in computational fluid dynamics is focused on the solution of the Navier-Stokes equations for increasingly complex airfoil and wing configurations. Some of the issues being examined in these solutions are the efficiency of the algorithms, the accuracy of the solutions, and the generation of grids for complex geometries. Cartesian grids are being pursued as a simple alternative to complicated grid generation techniques for general configurations. The successful implementation of Cartesian grids for the solution of the Euler equations[1] demonstrated the simplicity and utility of these grids, especially when multi-element configurations were considered. More recently, use of Cartesian grids was extended to the solution of the Euler equations for flowfields around three-dimensional geometries.[2]

The goal of the present work is to show the feasibility of using Cartesian grids in the solution of the Navier-Stokes equations for complex two-dimensional configurations. Because of the many issues that were uncovered by the investigation, it was decided to limit the scope of the paper to laminar flows. The algorithm employed is similar to that used in Refs. 1 and 2 and is based on the explicit Runge-Kutta time-stepping scheme of Jameson et al.[3] Modifications pertaining to numerical damping were examined. Moreover, the crucial influence of surface cells on the pressure and skin friction is investigated in detail.

A cell-centered scheme is employed. For such a scheme it is necessary to estimate the pressure and the various components of the stress tensor and the heat flux vector at the wall. The wall pressure was estimated by extrapolation.[1,2] Two different methods for determining wall stresses are used, and their effect on the solution is discussed.

In addition to the solution of the full equations, two simplified versions of the governing equations are considered. The results are compared with those of Swanson and Turkel[4] and Rumsey et al.[5] In general, good agreement is indicated when smoothly varying surface grids are employed.

Received July 20, 1987; revision received Dec. 1, 1987.

*Research Assistant, Mechanical and Aerospace Engineering.
†Professor, Mechanical and Aerospace Engineering. Associate Fellow AIAA.
‡Head, Theoretical Aerodynamics Branch, Transonic Aerodynamics Division. Associate Fellow AIAA.

Formulation of the Problem

A. Governing Equations

The conservation law form of the compressible Navier-Stokes equations in two dimensions can be written as

$$\frac{\partial W}{\partial t}+\frac{\partial F}{\partial x}+\frac{\partial G}{\partial y}=0 \tag{1}$$

where x and y are the Cartesian coordinates, and

$$W=[\rho,\rho u,\rho v,\rho E]^t \tag{2a}$$

$$F=[\rho u,\rho u^2+p-\sigma_{xx},\rho uv-\sigma_{xy},\rho uH - u\sigma_{xx}-v\sigma_{xy}+q_x]^t \tag{2b}$$

$$G=[\rho v,\rho uv-\sigma_{xy},\rho v^2+p-\sigma_{yy},\rho vH - u\sigma_{xy}-v\sigma_{yy}+q_y]^t \tag{2c}$$

In Eqs. (2), ρ is the density, p is the pressure, E and H are the total energy and enthalpy per unit mass, u and v are the velocity componets in the x and y directions, σ_{ij} is the stress tensor, and q_i is the heat flux vector. For a perfect gas, the equation of state is

$$p=R\rho T \tag{3}$$

where R is the gas constant, and T is the temperature. The thermodynamic variables are related by the expressions

$$E=[p/(\gamma-1)\rho]+\tfrac{1}{2}(u^2+v^2) \tag{4a}$$

$$H=E+(p/\rho) \tag{4b}$$

where γ is the ratio of specific heats. Using index notation, the stress tensor for a Newtonian fluid may be written as

$$\sigma_{ij}=\mu\left[\frac{\partial u_i}{\partial x_j}+\frac{\partial u_j}{\partial x_i}+\left(\frac{\theta}{\mu}-\frac{2}{3}\right)\delta_{ij}\frac{\partial u_m}{\partial x_m}\right] \tag{5}$$

where δ_{ij} is the Kronecker delta ($\delta_{ij} = 1$ if $i = j$ and zero otherwise), μ is the coefficient of shear viscosity, and θ is the coefficient of bulk viscosity and is assumed zero. When Fourier's law of heat conduction is assumed, the heat flux vector can be expressed as

$$q_i = -\lambda_t \frac{\partial T}{\partial x_i} \tag{6}$$

where λ_t is the coefficient of thermal conductivity.

The integral of Eq. (1) for a region Ω with a boundary $\partial\Omega$ can be written as

$$\frac{\partial}{\partial t}\int_\Omega W\,dA + \int_{\partial\Omega}(F\,dy - G\,dx) = 0 \tag{7}$$

Both F and G have inviscid and viscous components. Referring to the cell shown in Fig. 1, the inviscid component can be integrated in the manner indicated in Ref. 1. The manner in which the viscous terms are integrated is illustrated by the integration of the viscous terms in the x-momentum equation along side 3 of Fig. 1. The result for a cell-centered scheme takes the form

$$\begin{aligned}\int(-\sigma_{xx}\,dy + \sigma_{xy}\,dx) &= -\frac{2}{3}\int\mu\left(2\frac{\partial u}{\partial x} - \frac{\partial v}{\partial y}\right)dy \\ &+ \int\mu\left(\frac{\partial u}{\partial y} + \frac{\partial v}{\partial x}\right)dy \\ &= \mu_a\left[\frac{4}{3}(u_{i+1,j} - u_{i,j})\frac{\Delta v}{\Delta x} - \frac{2}{3}(v_D - v_C)\right. \\ &\left. + u_D - u_C + (v_{i+1,j} - v_{i,j})\frac{\Delta y}{\Delta x}\right]\end{aligned} \tag{8}$$

where u_C and u_D are calculated from

$$u_D = \tfrac{1}{4}(u_{i,j+1} + u_{i+1,j+1} + u_{i,j} + u_{i+1,j}) \tag{9a}$$

$$u_C = \tfrac{1}{4}(u_{i,j} + u_{i+1,j} + u_{i,j-1} + u_{i+1,j-1}) \tag{9b}$$

$$\mu_a = \tfrac{1}{2}(\mu_{ij} + \mu_{i+1,j}), \qquad \Delta x = x_{i+1} - x_i \tag{9c}$$

As a result of the above operations, the governing equation for cell (i, j) can be written as

$$\frac{dW_{ij}}{dt} + \frac{Q_{ij}}{A_{ij}} = 0, \qquad Q_{ij} = \int_{\partial\Omega}(F\,dy - G\,dx)_{ij} \tag{10}$$

For a Cartesian grid with equal cells, the above representation corresponds to central differencing. To suppress odd-even point decoupling and to prevent oscillations in the solution around regions of high gradients, numerical dissipation terms are added to the above equation. As a result, Eq. (10) is replaced by

$$\frac{dW_{ij}}{dt} + \frac{1}{A_{ij}} + (Q_{ij} - D_{ij}) = 0 \tag{11}$$

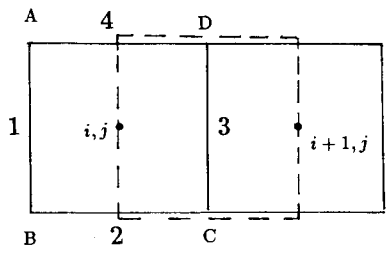

Fig. 1 Typical cell for Cartesian grids.

where D_{ij} is the dissipation term and is represented by

$$D_{ij} = Dx + Dy$$

with

$$Dx = d_{i+\frac{1}{2},j} - d_{i-\frac{1}{2},j} \tag{12a}$$

$$Dy = d_{i,j} + \tfrac{1}{2} - d_{i,j-\frac{1}{2}} \tag{12b}$$

One form of $d_{i+\frac{1}{2},j}$ employed in this work is taken from Ref. 3, i.e.,

$$\begin{aligned}d_{i+\frac{1}{2},j} = \frac{A_{i+\frac{1}{2},j}}{\Delta t}\,[&\epsilon^{(2)}_{i+\frac{1}{2},j}(w_{i+1,j} - w_{i,j}) \\ &- \epsilon^{(4)}_{i+\frac{1}{2},j}(w_{i+2,j} - 3w_{i+1,j} + 3w_{i,j} - w_{i-1,j})]\end{aligned} \tag{13}$$

where

$$\frac{1}{\Delta t} = \frac{1}{\Delta t_x} + \frac{1}{\Delta t_y} \tag{14a}$$

$$\Delta t_x = \frac{CFL\,\Delta x}{\lambda_x} \tag{14b}$$

$$\Delta t_y = \frac{CFL\,\Delta y}{\lambda_y} \tag{14c}$$

The coefficients $\epsilon^{(2)}$ and $\epsilon^{(4)}$ depend on the local pressure gradient; CFL is the Courant number, and λ is the maximum eigenvalue. Another form of $d_{i+\frac{1}{2},j}$ implemented here follows from Eq. (13) by replacing Δt by Δt_x with similar adjustment for $d_{i,j+\frac{1}{2}}$.

B. Boundary Conditions

The conditions at the inflow boundary normal to the x-axis and the far-field boundaries normal to the y-axis are those appropriate for the Euler equation and are derived from the theory of characteristics.[1] At the outflow boundary normal to the x-axis, all of the flow properties are extrapolated from the interior.

A no-slip boundary condition is implemented on the surface of a solid boundary. It is necessary, when employing a cell-centered scheme, to calculate the stresses, the heat flux, and the pressure at the wall. The pressure was calculated by extrapolation.[1] Two different procedures were used to calculate the stresses. In the first, the velocity in a cell adjacent to the wall is assumed to have the representation

$$u = a + bx + cy \tag{15}$$

where a, b, and c are cell-dependent quantities. They are determined in terms of the value of u at the cell center and the value of u (which is zero) at the points where the cell intersects the wall. The values of $\partial u/\partial x$ and $\partial u/\partial y$ at the wall are then given as b and c. Similar procedure is used to determine $\partial v/\partial x$ and $\partial v/\partial y$.

In the second method, the velocity near the surface is assumed to be quadratic. Thus, in order to determine $\partial u/\partial y$ at the wall, u is assumed to have the representation

$$u = a + by + cy^2 \tag{16}$$

where, again, a, b, and c are cell-dependent quantities. The zero velocity at the wall and the velocities at the two adjacent cells are used to determine a, b, and c. The desired derivative follows as

$$\frac{\partial u}{\partial y} = b + 2cy_b \tag{17}$$

where y_b is the value of y at the body surface. Similar procedure is used to determine the remaining derivatives at the wall. Adiabatic wall conditions were assumed, thus $q_w = 0$.

C. Transport Properties

The shear viscosity is calculated from the relation

$$\frac{\mu}{\mu_\infty} = \frac{T}{T_\infty} \tag{18}$$

where subscript infinity denotes the freestream conditions. The coefficient of thermal conductivity is determined by specifying the Prandtl number Pr

$$Pr = \frac{\mu C_p}{\lambda_t} = \frac{\gamma}{\gamma - 1}\frac{\mu R}{\lambda_t} \tag{19}$$

where C_p is the specific heat at constant pressure. A value of $Pr = 0.72$ is used in this work.

D. Method of Solution

The explicit four-stage Runge-Kutta time-stepping scheme of Jameson et al.,[3] is employed. In order to accelerate convergence to the steady state, each cell is stepped locally at its own maximum allowable time step. Implicit residual smoothing[6] was employed to accelerate convergence to the steady state.

Results and Discussion

In order to bring out the problems that can arise when using Cartesian grids in the solution of the Navier-Stokes equations, the laminar flow over a NACA 0012 airfoil is considered first. The Reynolds, Mach, and Prandtl numbers are 5000, 0.5, and 0.72, respectively, while the angle of attack is zero. With the exception of the Prandtl number, this case was computed by Swanson and Turkel[4] using a 128×64 C-grid. The thin-layer approximation was employed in Ref. 4. The 129×71 Cartesian grid chosen is shown in Fig. 2. The minimum Δy was 3×10^{-3}. This spacing was maintained constant over the entire thickness of the body in order to provide sufficient resolution in the boundary layer. All boundaries were placed at five chord lengths away from the body. This grid will be referred to as the initial grid.

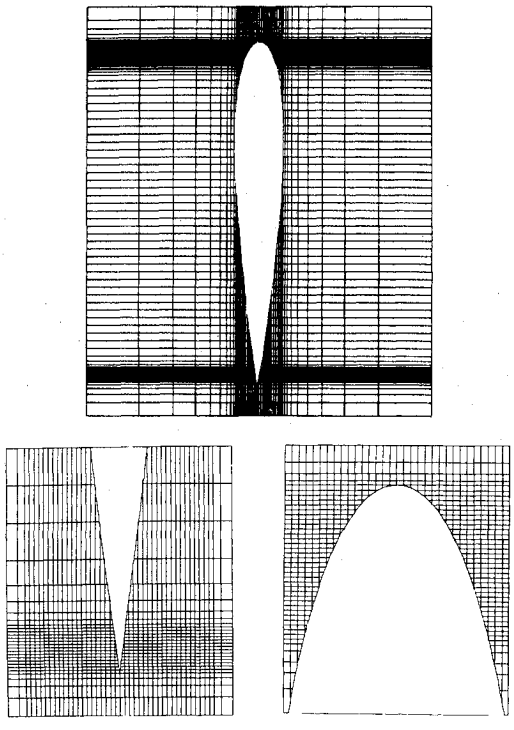

Fig. 2 Initial Cartesian grid for NACA 0012.

As was pointed out in Ref. 1, use of Cartesian grids for bodies of arbitrary shapes may result in surface cells with widely varying areas. This will produce, in certain extreme cases, a nonuniform wall pressure distribution. In order to limit the size difference, surface cells whose areas are below a specified percentage (50% or less) of the uncut cell are incorporated into adjacent cells away from the body. This practice was followed here.

Calculations based on the full Navier-Stokes equations were carried out for the conditions indicated above. The results for the pressure and skin-friction coefficients are compared with those of Ref. 4 in Fig. 3. It is seen from the figure that the agreement is rather poor. Attempts at improving the agreement involved grid refinement, various ways of extrapolation of surface properties, and various forms of numerical smoothing. None of the above attempts made any tangible difference.

Grid Smoothness

After exhausting all other possibilities, attention was directed to the grid employed. Examination of the initial grid showed that it contained an assortment of polygonal and

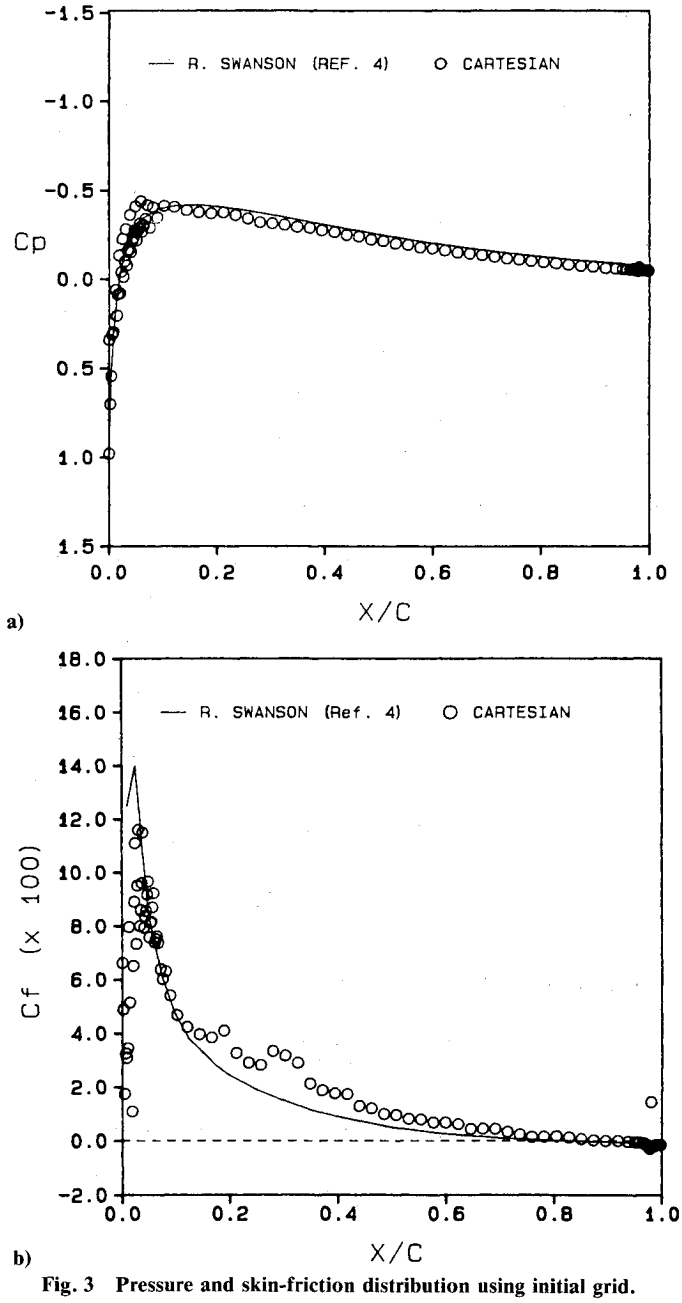

Fig. 3 Pressure and skin-friction distribution using initial grid.

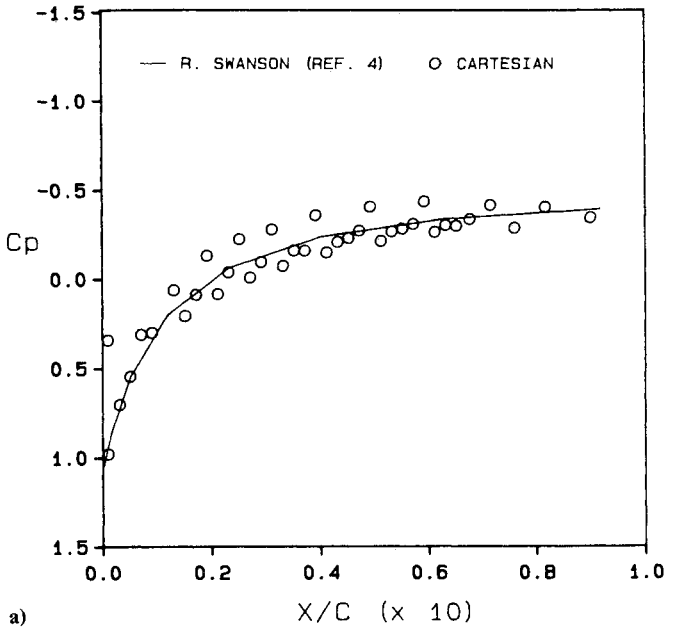

a)

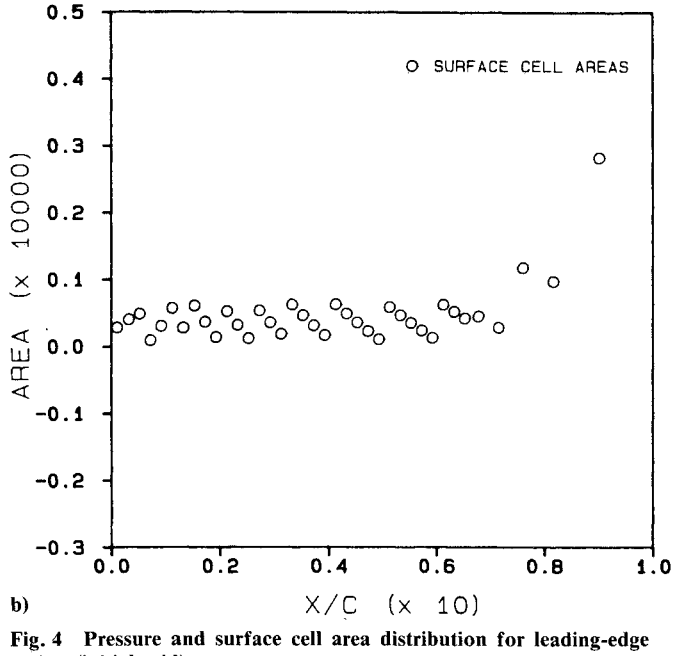

b)

Fig. 4 Pressure and surface cell area distribution for leading-edge region (initial grid).

triangular surface cells whose areas were randomly distributed. The role played by the grid is seen in Fig. 4, which shows an enlargement of the pressure coefficient distribution and the areas of surface cells around the leading edge. As is seen from the figure, the pressure fluctuation correlates well with the area fluctuation. In particular, regions where a large cell is adjacent to a small cell correspond to regions where there is the largest deviation of the pressure coefficient from the results of Ref. 4.

A grid of 109 × 71 then was created (to be referred to as the intermediate grid) so that the x and y grid lines intersected at the airfoil surface for the front part of the airfoil without disturbing the remaining grid, shown in Fig. 2. This construction ensures the smooth variation of surface cells. A closeup of the leading-edge region and the distribution of areas of surface cells are shown in Fig. 5. The results of the computations are shown in Fig. 6. As is seen from the figure, the new grid resulted in a smooth pressure distribution, but the skin friction distribution is nonuniform over the aft portion of the airfoil.

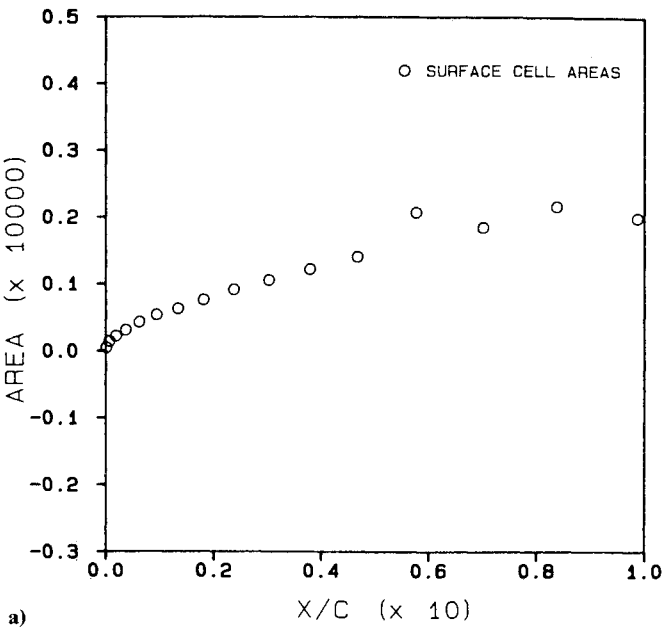

a)

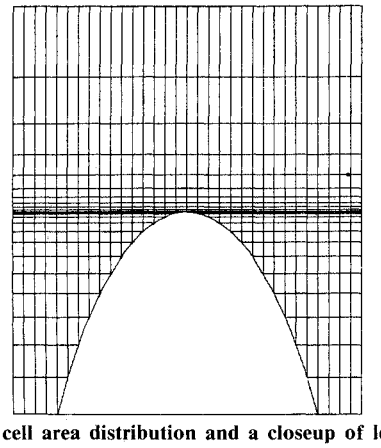

b)

Fig. 5 Surface cell area distribution and a closeup of leading-edge region (intermediate grid).

Next, an 89 × 89 grid was generated with smoothly varying surface areas for the entire length of the airfoil. The front and side boundaries were placed five chords away from the body, while the downstream boundary extended six chord lengths behind the body. A closeup of the grid is shown in Fig. 7. All subsequent calculations for the NACA 0012 airfoil employed this grid.

Figure 8 compares the pressure and skin friction with those of Ref. 4. Surface stresses were estimated using a procedure based on Eq. (15). With the exception of the value of C_f at the leading edge, reasonable agreement is indicated. The results in Fig. 8 were obtained after 3000 iterations and correspond to a six-order reduction in the residual.

Stresses and Their Extrapolation

The influence of the normal and the shear stresses and procedures used for their extrapolation on the skin friction are considered next. In the first, σ_{xx}, σ_{yy}, and q_x are neglected, and σ_{xy} is retained. In the second, the above assumptions are supplemented by the approximation $\sigma_{xy} = \mu(\partial u/\partial y)$. Figures 9 and 10 show the effects of such approximation on the pressure and skin-friction distributions. As is seen from these figures, the influence of these simplifications is essentially limited to the skin friction around the leading edge. Figure 10, which is based on the assumption that $\sigma_{xx} = \sigma_{yy} = q_x = 0$, gives the best agreement with the results of Ref. 4. The results of Ref. 4 ignore viscous terms involving gradients parallel to the sur-

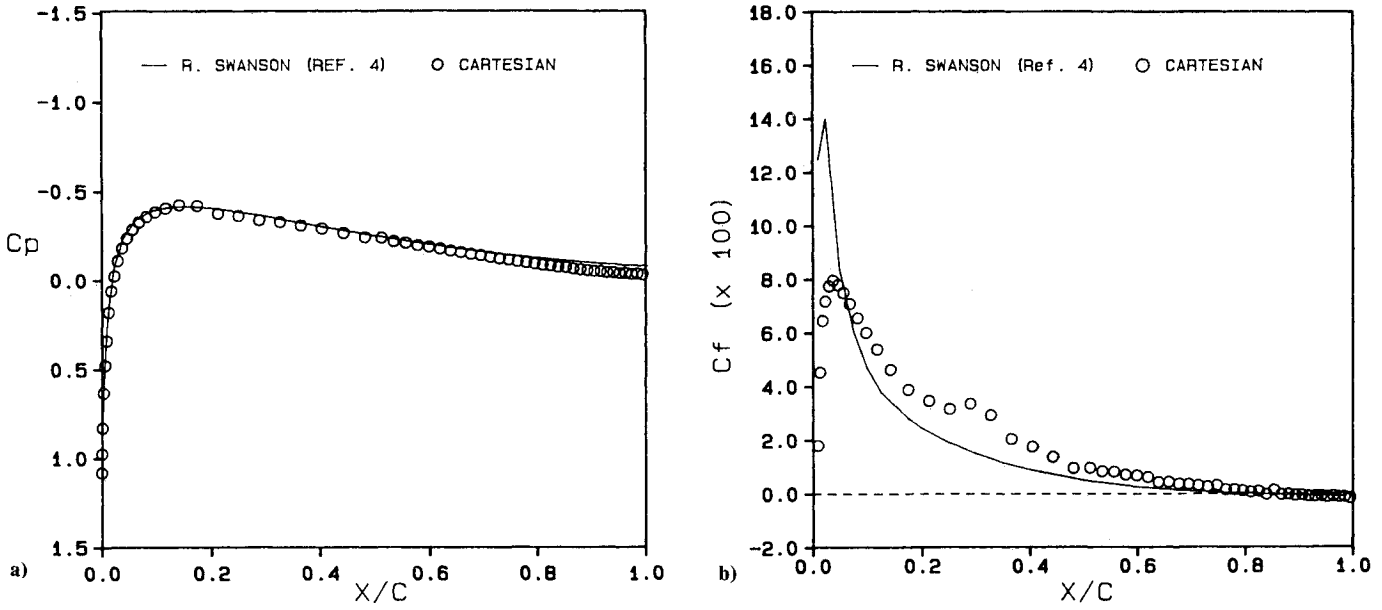

Fig. 6 Pressure and skin-friction distribution on intermediate grid.

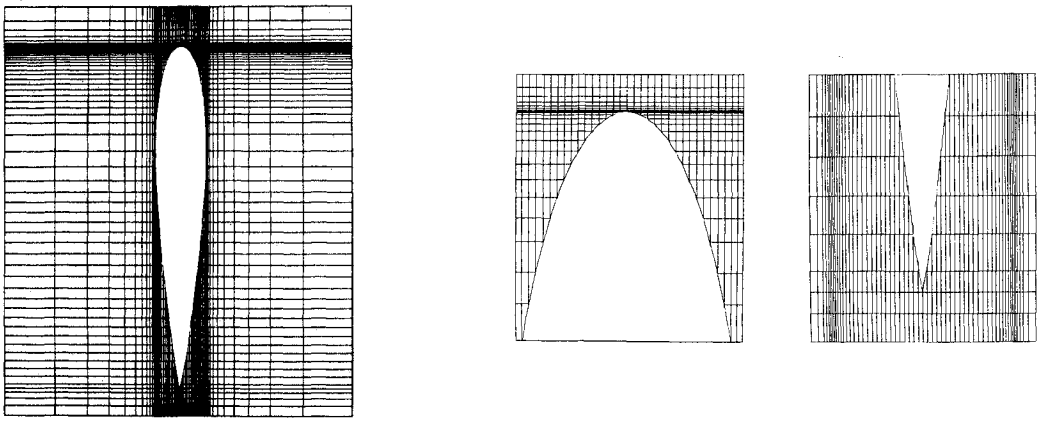

Fig. 7 Final Cartesian grid (89 × 89).

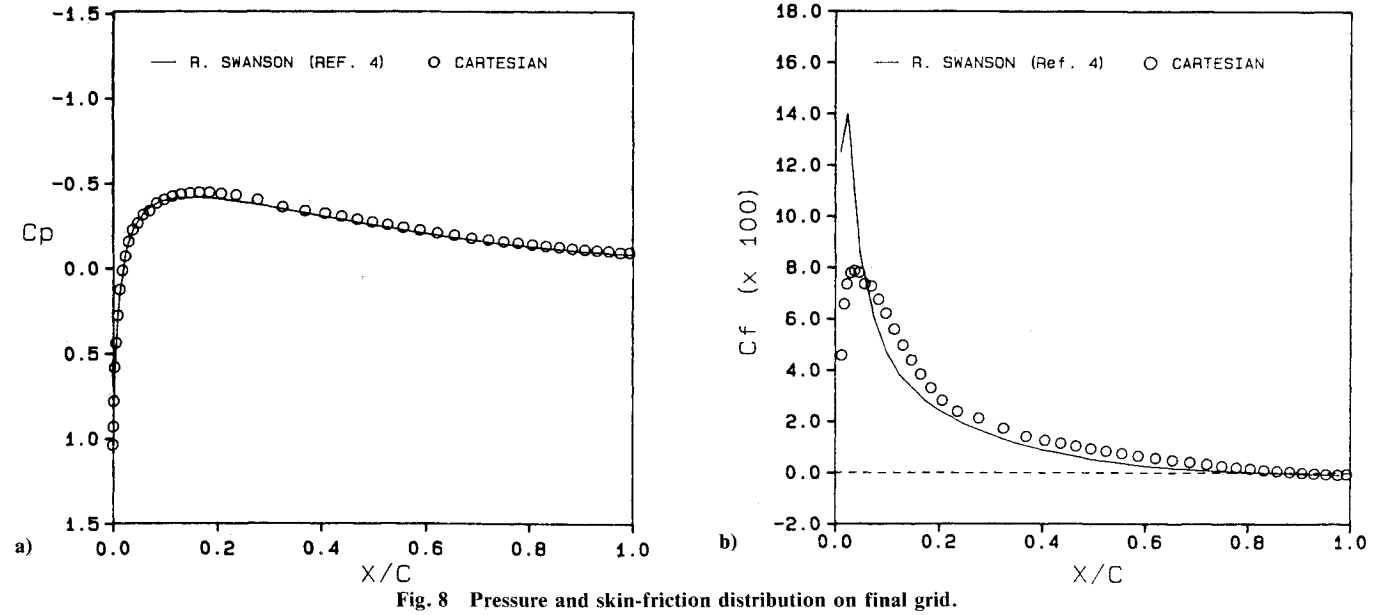

Fig. 8 Pressure and skin-friction distribution on final grid.

face. Evidently, the assumptions used to obtain the results of Fig. 10 are good approximation to the assumptions used in Ref. 4. Note also that neither of the simplifications affect the location of the point of separation.

In all of the above results, stress calculations on the wall were based on the linear velocity representation indicated in Eq. (15). Figure 11 shows the effect of using the quadratic representation given by Eq. (16). Comparing the results in Fig. 11 with these in Fig. 8 shows that the quadratic representation yields better agreement with the results of Ref. 4.

The above results also illustrate the insensitivity of the pressure distribution to simplifications in the governing

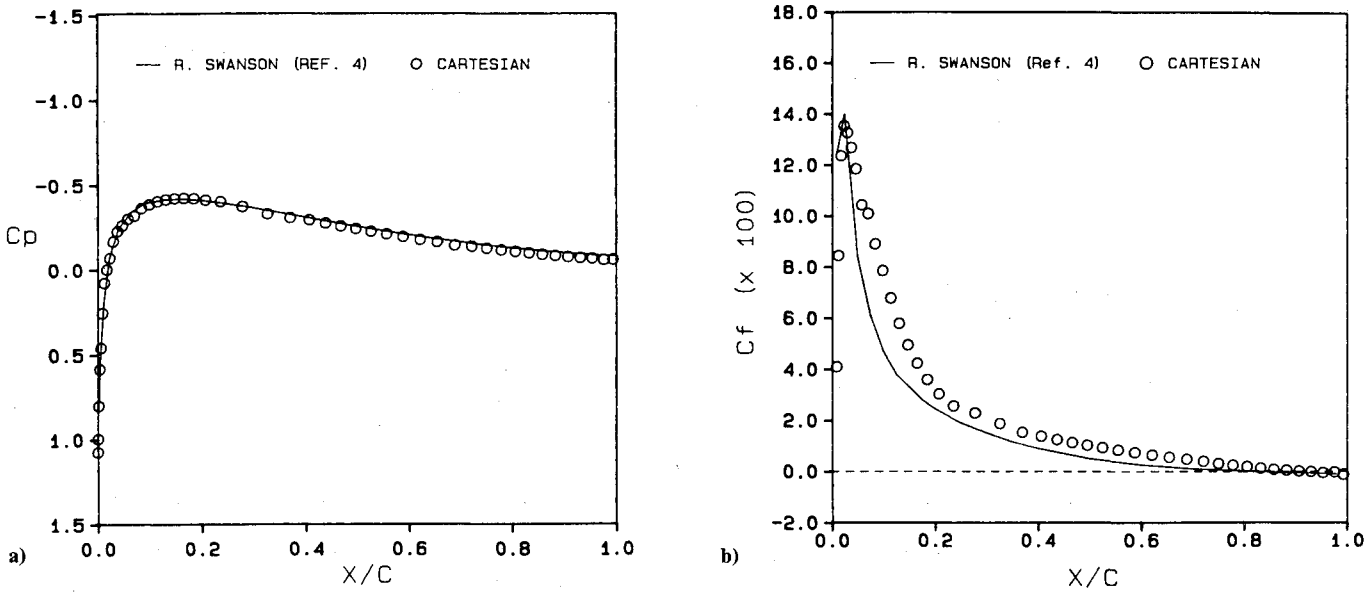

Fig. 9 Effect of first thin-layer approximation on pressure and skin friction.

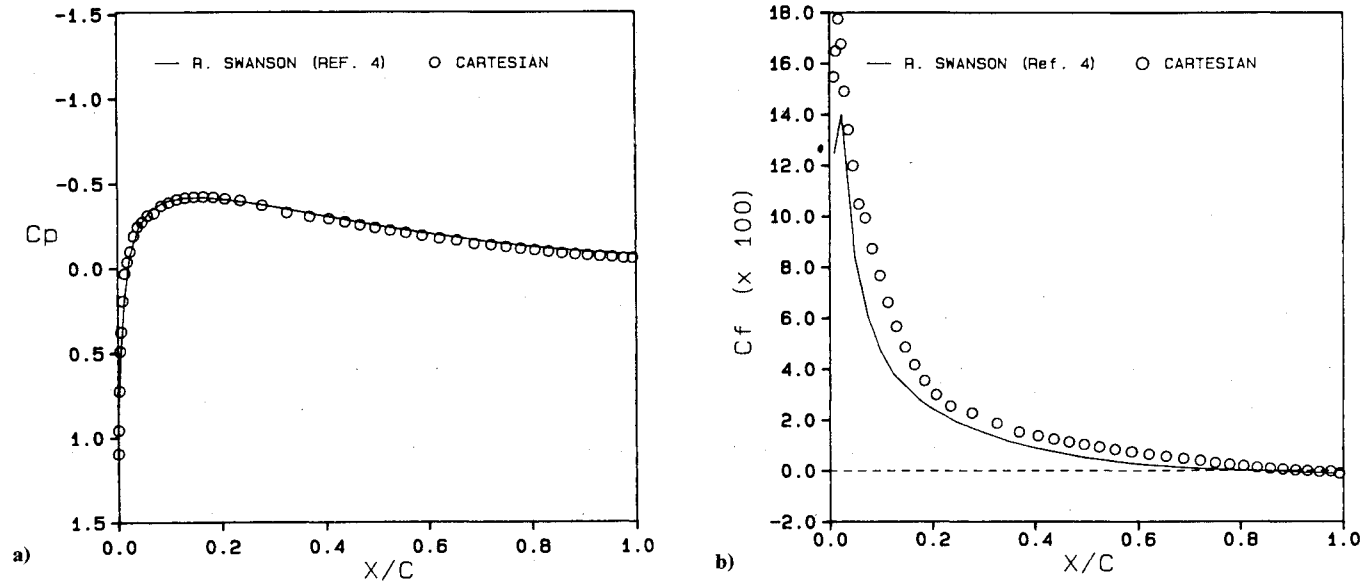

Fig. 10 Effect of second thin-layer approximation on pressure and skin friction.

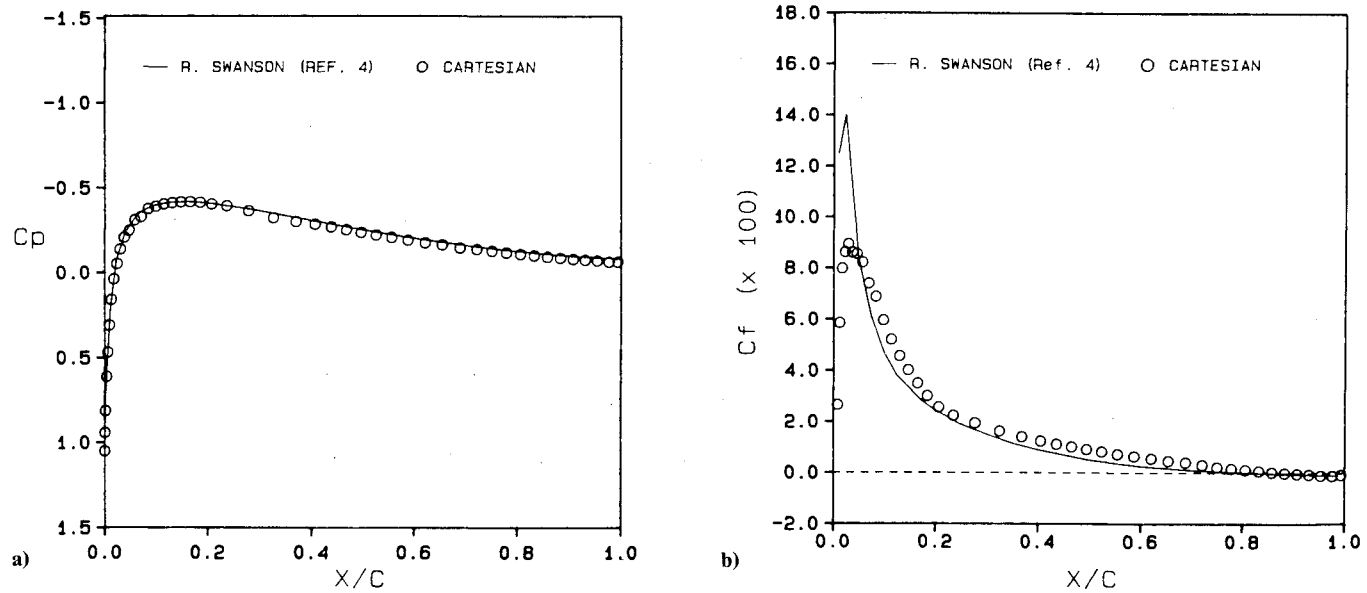

Fig. 11 Effect of second-order extrapolation on pressure and skin friction.

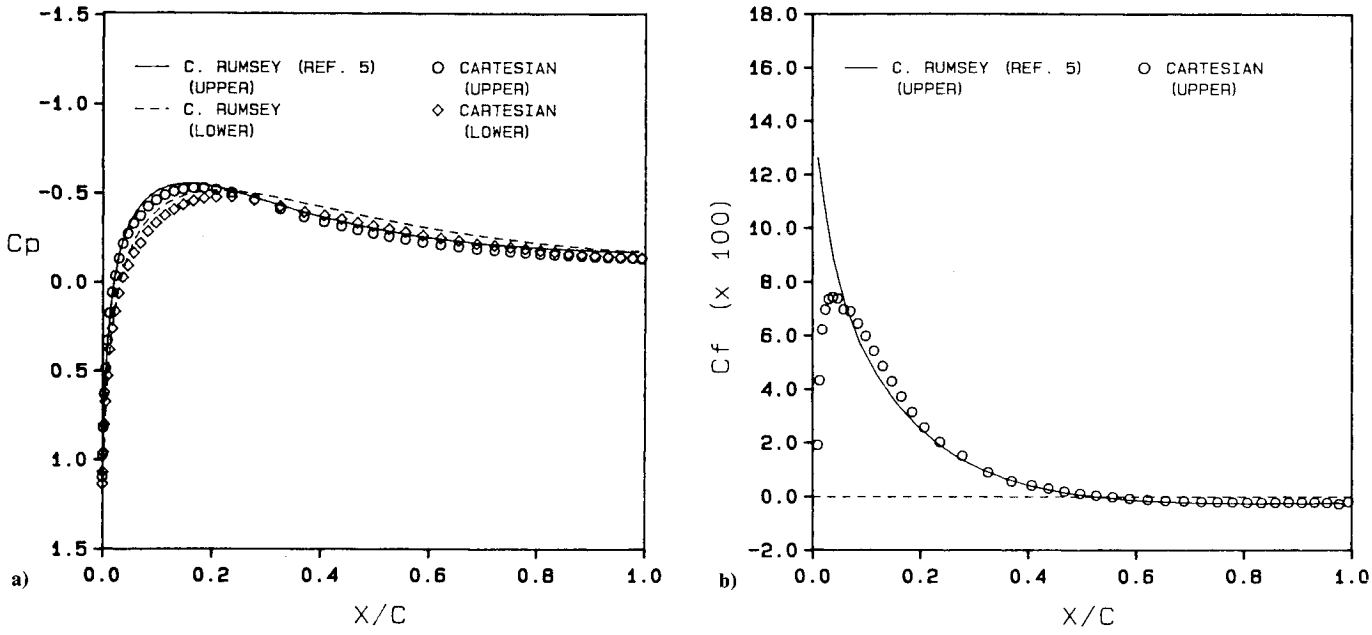

Fig. 12 Pressure and skin-friction distribution for NACA 0012 at $M = 0.758$ and $\alpha = 1$ deg.

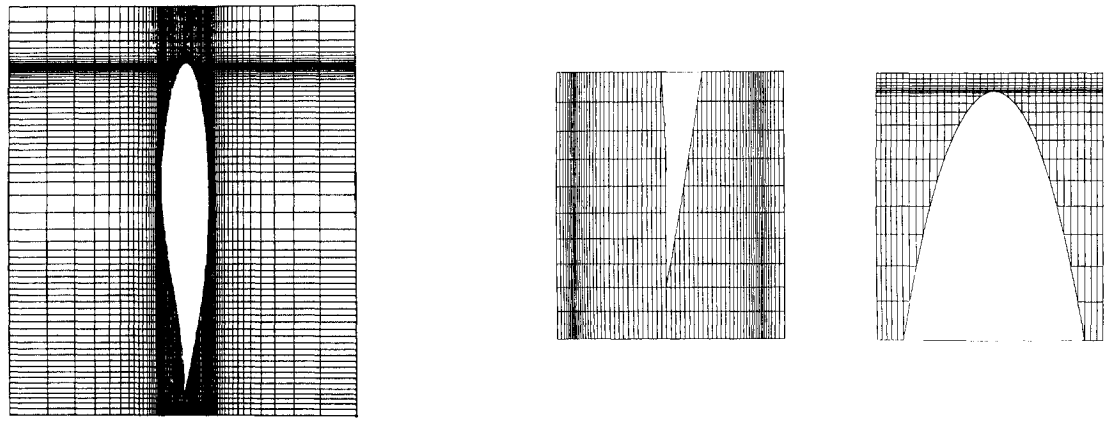

Fig. 13 Cartesian grid for RAE 2822.

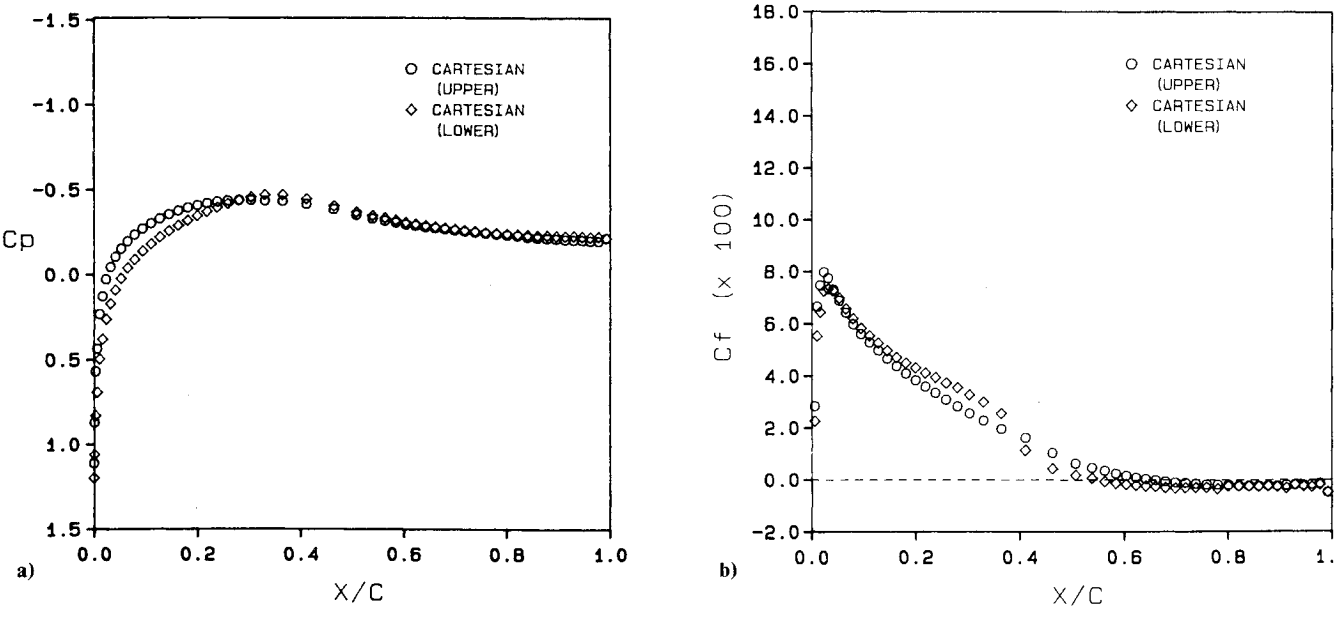

Fig. 14 Pressure and skin-friction distribution for RAE 2822 at $M = 0.8$ and $\alpha = 1$ deg.

equations and to the method of evaluating the wall shear stress. This suggests that accuracy of Navier-Stokes solutions should not be judged solely on comparisons with pressure distributions.

Numerical Smoothing

All of the above results used the numerical smoothing indicated in Eq. (13). The expressions for $\epsilon^{(2)}$ and $\epsilon^{(4)}$ were identical to those used for the Euler calculations.[1,3] Minor improvements were noted when Δt_x and Δt_y replaced Δt in the expressions for $d_{i+\frac{1}{2},j}$ and $d_{i,j+\frac{1}{2}}$. This is because the aspect ratios of the surface cells were within a factor of ten.

Flow Asymmetry

The above calculations were carried out for a symmetric airfoil at zero angle of attack. The remaining results demonstrate the approach for symmetric airfoils at incidence and for nonsymmetric airfoils. It should be emphasized that consideration of such flows does not require any new logic in the code. Figure 12 presents skin-friction coefficient and pressure distribution for a NACA 0012 at a freestream Mach number of 0.758, an angle of attack of 1 deg, and a Reynolds number of 5000. The results are compared with calculations using the implicit upwind code of Rumsey et al.[5] The code is based on van Leer's flux vector splitting scheme. Rumsey's calculation used a 191×59 C-grid. Again, reasonable agreement is indicated.

The final set of calculations dealt with the RAE 2822, a nonsymmetric airfoil. A closeup of the 113×117 grid employed is shown in Fig. 13. Figure 14 shows a representative calculation for pressure coefficient and skin friction for a Mach number of 0.8, a Reynolds number of 5000, and an angle of attack at 1 deg. The smoothness of the results indicates that a smoothly varying grid can be generated for such an airfoil.

Concluding Remarks

Use of Cartesian grids in conjunction with complex shapes results in a variety of polygonal and triangular surface cells with randomly distributed areas. Calculations using such grids were successfully demonstrated earlier for the Euler equations. This work demonstrates that Cartesian grids can be used for the solution of the Navier-Stokes equations for two-dimensional bodies of complex shapes, provided the surface cells have smoothly varying areas. This feature of the grid is more important than cell aspect ratio or cell size. It would be desirable to quantify the measure of surface grid smoothness, but this is not an easy problem.

Results indicate that agreement with the pressure distribution does not guarantee good agreement with the skin friction. Thus, the quality and accuracy of Navier-Stokes solutions should be judged based on comparisons with skin friction and heat-transfer measurements and not on pressure measurements.

Two simplifications of the Navier-Stokes equations were considered. The first was based on the assumption that $\sigma_{xx} = \sigma_{yy} = q_x = 0$. The second assumed, in addition to the above, that $\sigma_{xy} = \mu(\partial u/\partial y)$. The pressure distribution was found to be insensitive to these simplifications, but the skin friction around the leading edge was. Moreover, the first simplification gave best agreement with codes using the thin-layer approximation and body-fitted grids.

Acknowledgment

The work was supported in part by NASA Cooperative Agreement NCC1-22. The authors would like to acknowledge many helpful discussions with Dr. R. C. Swanson and C. L. Rumsey of the NASA Langley Research Center.

References

[1]Clarke, D. K., Salas, M. D., and Hassan, H. A., "Euler Calculations for Multielement Airfoils Using Cartesian Grids," *AIAA Journal,* Vol. 24, March 1986, pp. 353–358.

[2]Gaffney, R. L., Salas, M. D., and Hassan, H. A., "Euler Calculations for Wings Using Cartesian Grids," AIAA Paper 87-0356, Jan. 1987.

[3]Jameson, A., Schmidt, W., and Turkel, E., "Numerical Solutions of the Euler Equations by Finite Volume Methods Using Runge-Kutta Time Stepping Schemes," AIAA Paper 81-1251, June 1981.

[4]Swanson, R. C. and Turkel, E., "A Multistage Time-Stepping Scheme for the Navier-Stokes Equations," AIAA Paper 85-0035, Jan. 1985.

[5]Rumsey, C. L., Thomas, J. L., Warren, G. P., and Liu, G. C., "Upwind Navier-Stokes Solutions for Separated Periodic Flows," AIAA Paper 86-0247, Jan. 1986.

[6]Jameson, A. and Baker, T. J., "Solutions of the Euler Equations for Complex Configurations," AIAA Paper 83-1929, July 1983.